

Supporting Information for

***In-Silico* Design of Copper-Based Alloys for Ammonia Synthesis
from Nitric Oxide Reduction Accelerated by Machine Learning**

Jie Feng, Yujin Ji^{1*}, and Youyong Li^{1,2*}

¹Institute of Functional Nano & Soft Materials (FUNSOM), Jiangsu Key Laboratory for Carbon-Based Functional Materials & Devices, Soochow University, Suzhou, Jiangsu 215123, China

²Macao Institute of Materials Science and Engineering, Macau University of Science and Technology, Taipa, Macau SAR 999078, China

*Corresponding author

Email address: yjji@suda.edu.cn (Y. Ji); yyli@suda.edu.cn (Y. Li);

Supplementary Notes

Note S1. The Introduction of ML algorithms

Scikit-Learn was used to obtain the KRR, MLP, RF, and GBDT algorithms which were chosen to build prediction models for comparing. Kernel ridge regression (KRR) is a combination of Ridge regression and classification with the kernel trick, thus learning a linear function in the space induced by the respective kernel and the data¹. Multi-layer Perceptron (MLP) is a supervised learning algorithm that learns a function $f(\cdot):R^m \rightarrow R^o$ by training on a dataset, where m is the number of dimensions for input and o is the number of dimensions for output². RF³ and GBDT⁴ are two sub-models of Decision Tree (DT) models⁵. To address the problem of overfitting that limits the application of DT, RF utilizes randomness injection into the tree building while GBDT tries to correct the mistakes of the previous tree continuously.

Note S2. The introduction of constructing bimetallic alloy surfaces

For a surface of copper alloy, we only consider the 18 nearest neighbors of active sites as the ML models are implemented based on these 18 atoms. To build bimetallic alloy surfaces, for every atom of these 18 atoms, we set it to Cu or X, where X = Fe, Co, Ni, Zn, Ru, Rh, Pd, Os, Ir, Pt. For example, if X = Fe, these 18 atoms can be Cu or Fe, and in total, 2^{18} (262144) CuFe bimetallic alloy surfaces are constructed. Hence, for the 10 metals, 2621440 bimetallic alloy surfaces are generated. Though there may exist the same surface due to the symmetry, we consider all the possibility as we aim to understand the optimal alloy element.

Supplementary Tables

Table S1 The specific hyperparameters of the four ML models.

	KRR	MLP	RF	GBDT
alpha	0.6	0.01		
hidden layer sizes		(150,150)		
learning rate		0.002		0.032
estimators			280	153
max depth			25	8
max features			126	126

Table S2. The all possible NORR pathways.

Name	Pathway
Distal-O	$* + \text{NO} + \text{H}^+ + \text{e}^- \rightarrow *\text{NOH}$ $*\text{NOH} + \text{H}^+ + \text{e}^- \rightarrow *\text{N} + \text{H}_2\text{O}$ $*\text{N} + \text{H}^+ + \text{e}^- \rightarrow *\text{NH}$ $*\text{NH} + \text{H}^+ + \text{e}^- \rightarrow *\text{NH}_2$ $*\text{NH}_2 + \text{H}^+ + \text{e}^- \rightarrow * + \text{NH}_3$
Distal-N	$* + \text{NO} + \text{H}^+ + \text{e}^- \rightarrow *\text{HNO}$ $*\text{HNO} + \text{H}^+ + \text{e}^- \rightarrow * \text{H}_2\text{NO}$ $* \text{H}_2\text{NO} + \text{H}^+ + \text{e}^- \rightarrow *\text{O} + \text{NH}_3$ $*\text{O} + \text{H}^+ + \text{e}^- \rightarrow *\text{OH}$ $*\text{OH} + \text{H}^+ + \text{e}^- \rightarrow * + \text{H}_2\text{O}$
Alternating-O	$* + \text{NO} + \text{H}^+ + \text{e}^- \rightarrow *\text{NOH}$ $*\text{NOH} + \text{H}^+ + \text{e}^- \rightarrow *\text{HNOH}$ $* \text{HNOH} + \text{H}^+ + \text{e}^- \rightarrow * \text{NH} + \text{H}_2\text{O}$ $*\text{NH} + \text{H}^+ + \text{e}^- \rightarrow *\text{NH}_2$ $*\text{NH}_2 + \text{H}^+ + \text{e}^- \rightarrow * + \text{NH}_3$
Alternating-N	$* + \text{NO} + \text{H}^+ + \text{e}^- \rightarrow *\text{HNO}$ $*\text{HNO} + \text{H}^+ + \text{e}^- \rightarrow *\text{HNOH}$ $* \text{HNOH} + \text{H}^+ + \text{e}^- \rightarrow * \text{H}_2\text{NOH}$ $* \text{H}_2\text{NOH} + \text{H}^+ + \text{e}^- \rightarrow * \text{NH}_2 + \text{H}_2\text{O}$ $*\text{NH}_2 + \text{H}^+ + \text{e}^- \rightarrow * + \text{NH}_3$

Table S3. Gibbs free binding energies of the NORR intermediates on different metal flat surfaces.

	$E_{\text{ads}}(\text{N})$	*NOH	*N	*NH	*NH ₂
Cu	1.93	0.32	-0.95	-1.96	-1.96
Cu ₃ Fe	0.65	-0.48	-2.24	-2.69	-2.92
Cu ₂ Fe ₂	0.26	-0.88	-2.63	-3.03	-2.70
Cu ₃ Co	0.76	-0.40	-2.11	-2.53	-2.72
Cu ₂ Co ₂	0.33	-0.82	-2.54	-2.94	-2.59
Cu ₃ Ni	1.16	-0.30	-1.71	-2.46	-2.70
Cu ₂ Ni ₂	0.37	-0.85	-2.49	-2.91	-2.97
Cu ₃ Zn	1.70	0.06	-1.18	-2.32	-2.52
Cu ₂ Zn ₂	1.36	-0.29	-1.52	-2.71	-2.60
Cu ₃ Ru	0.30	-0.49	-2.58	-2.55	-2.79
Cu ₂ Ru ₂	-0.02	-1.01	-2.90	-3.14	-3.02
Cu ₃ Rh	1.17	-0.07	-1.70	-2.05	-2.54
Cu ₂ Rh ₂	0.13	-0.79	-2.74	-2.85	-2.88
Cu ₃ Pd	1.85	0.16	-1.03	-1.96	-2.43
Cu ₂ Pd ₂	1.55	0.23	-1.32	-1.70	-2.20
CuOs ₃	0.01	-0.76	-2.88	-2.81	-2.99
Cu ₂ Os ₂	-0.12	-1.02	-2.99	-3.19	-3.02
CuIr ₃	0.78	-0.38	-2.10	-2.33	-2.76
Cu ₂ Ir ₂	0.06	-0.74	-2.81	-2.87	-2.87
CuPt ₃	1.49	0.07	-1.38	-2.06	-2.45
Cu ₂ Pt ₂	1.01	-0.11	-1.86	-2.08	-2.52

Table S4. The optimized intermediates for Cu, Cu@Cu₃Ni, and Cu₂Ni₂@Cu₃Ni.

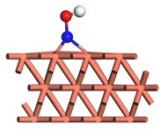
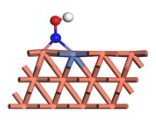
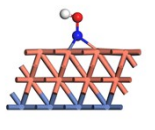
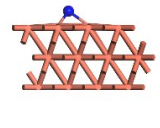
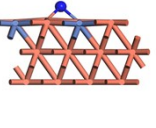
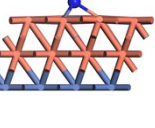
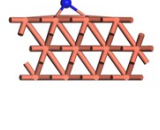
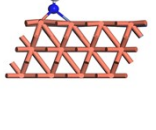
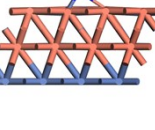
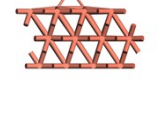
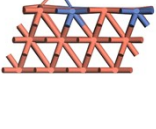
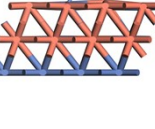
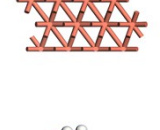
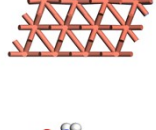
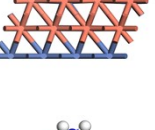
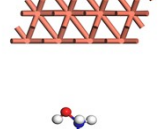
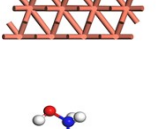
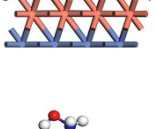
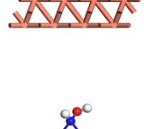
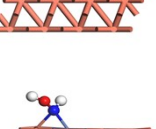
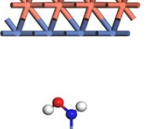
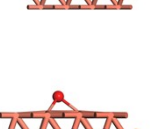
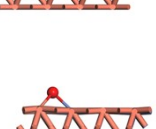
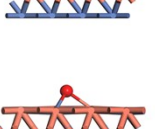
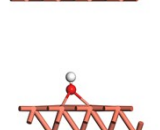
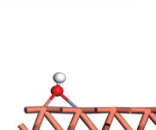
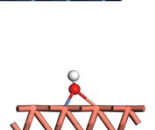
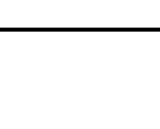
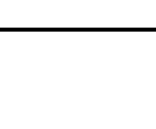
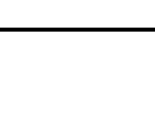
	Cu	Cu@Cu ₃ Ni	Cu ₂ Ni ₂ @Cu ₃ Ni
*NOH			
*N			
*NH			
*NH ₂			
*HNO			
*H ₂ NO			
*H ₂ NOH			
*HNOH			
*O			
*OH			

Table S5. Comparison of the competitive adsorption energies of NO and H₂O.

	NO	H ₂ O
Cu@Cu ₃ Ni	-0.18	-0.03
Cu ₂ Ni ₂ @Cu ₃ Ni	-0.38	-0.04

Supplementary Figures

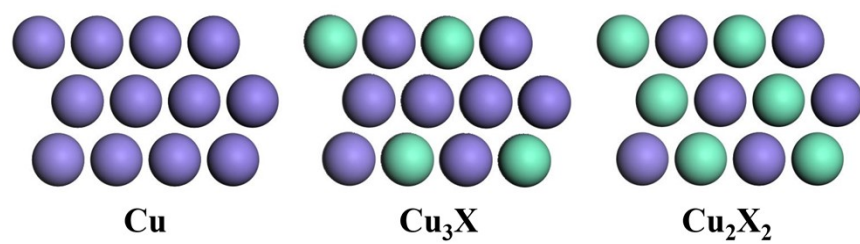


Figure S1. The geometric structures of Cu, Cu₃X, and Cu₂X₂ from the side view. The metal X and Cu atoms are marked by cyan and purple spheres, respectively.

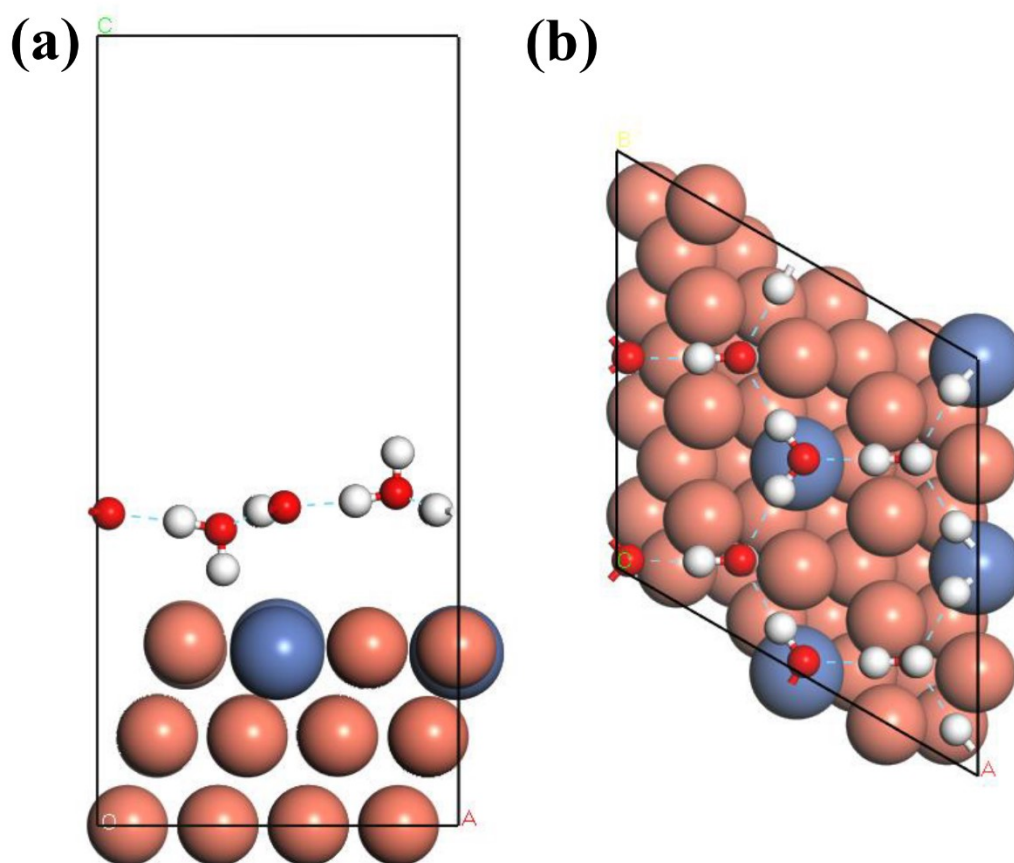


Figure S2. Side (a) and top (b) view of the optimized model of electrochemical solid-liquid interface on Cu@Cu₃Ni. The light red, red, white and blue atom represent Cu, O, H and Ni. The dash line represents H-bond network.

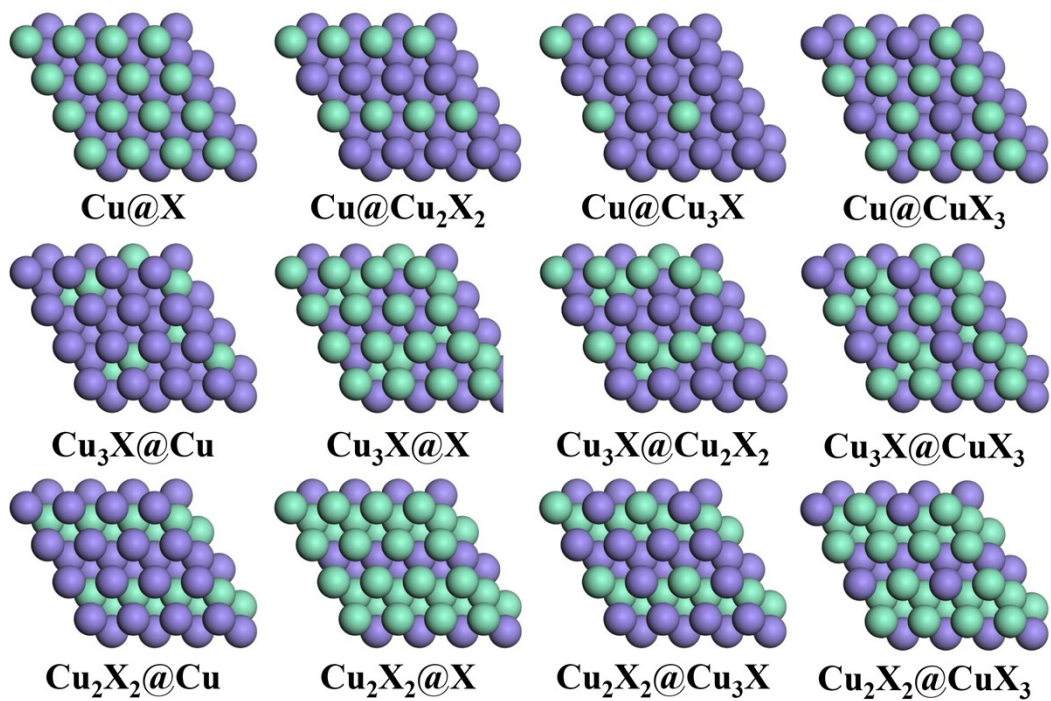


Figure S3. The geometric structures of the copper based alloys from the top view. The metal X and Cu atoms are marked by cyan and purple spheres, respectively.

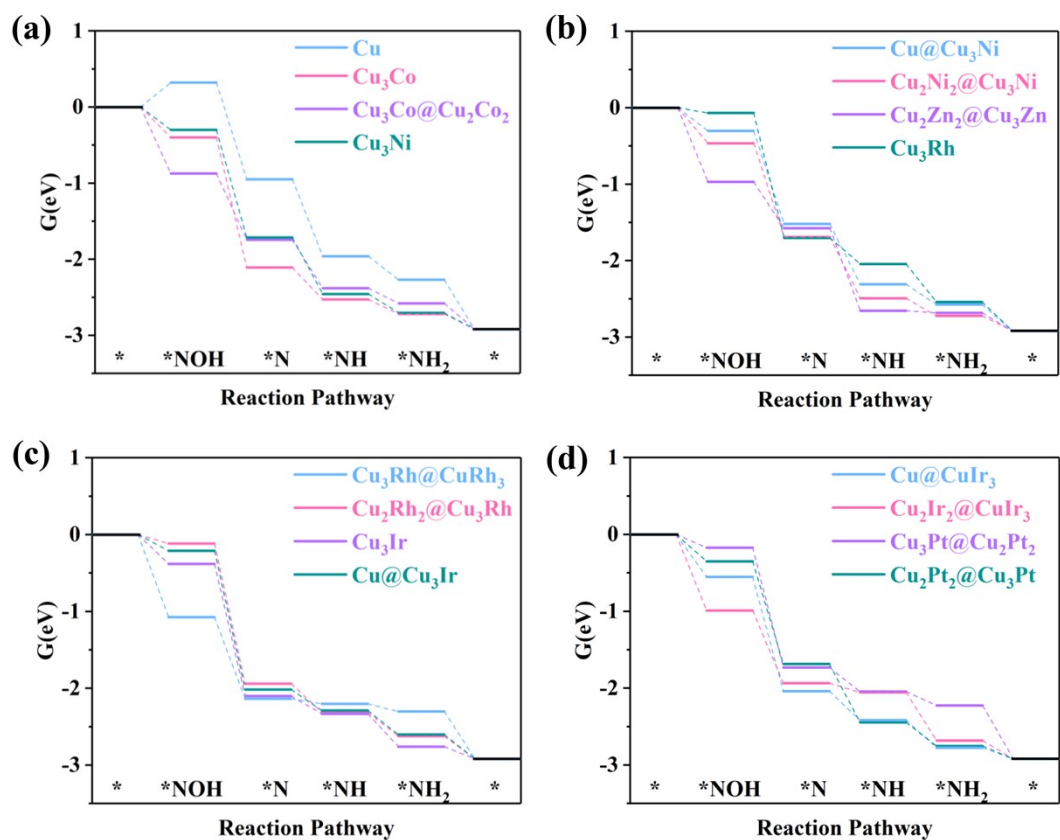


Figure S4. The Distal-O reaction pathway for the 15 select alloys.

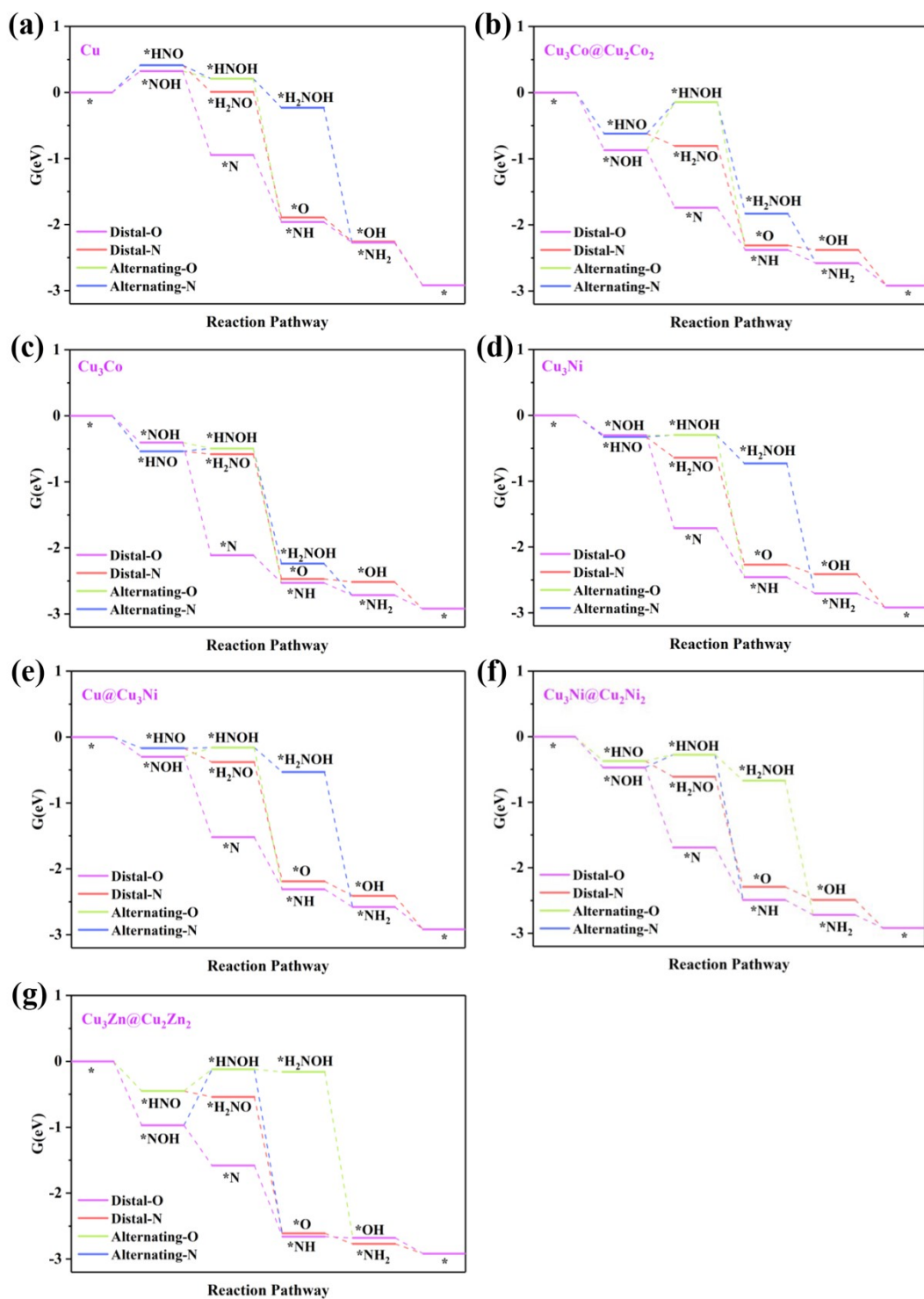


Figure S5. The all possible reaction pathways for Cu, Cu₃Co, Cu₃Ni, Cu₃Co@Cu₂Co₂, Cu@Cu₃Ni, Cu₂Ni₂@Cu₃Ni, and Cu₂Zn₂@Cu₃Zn.

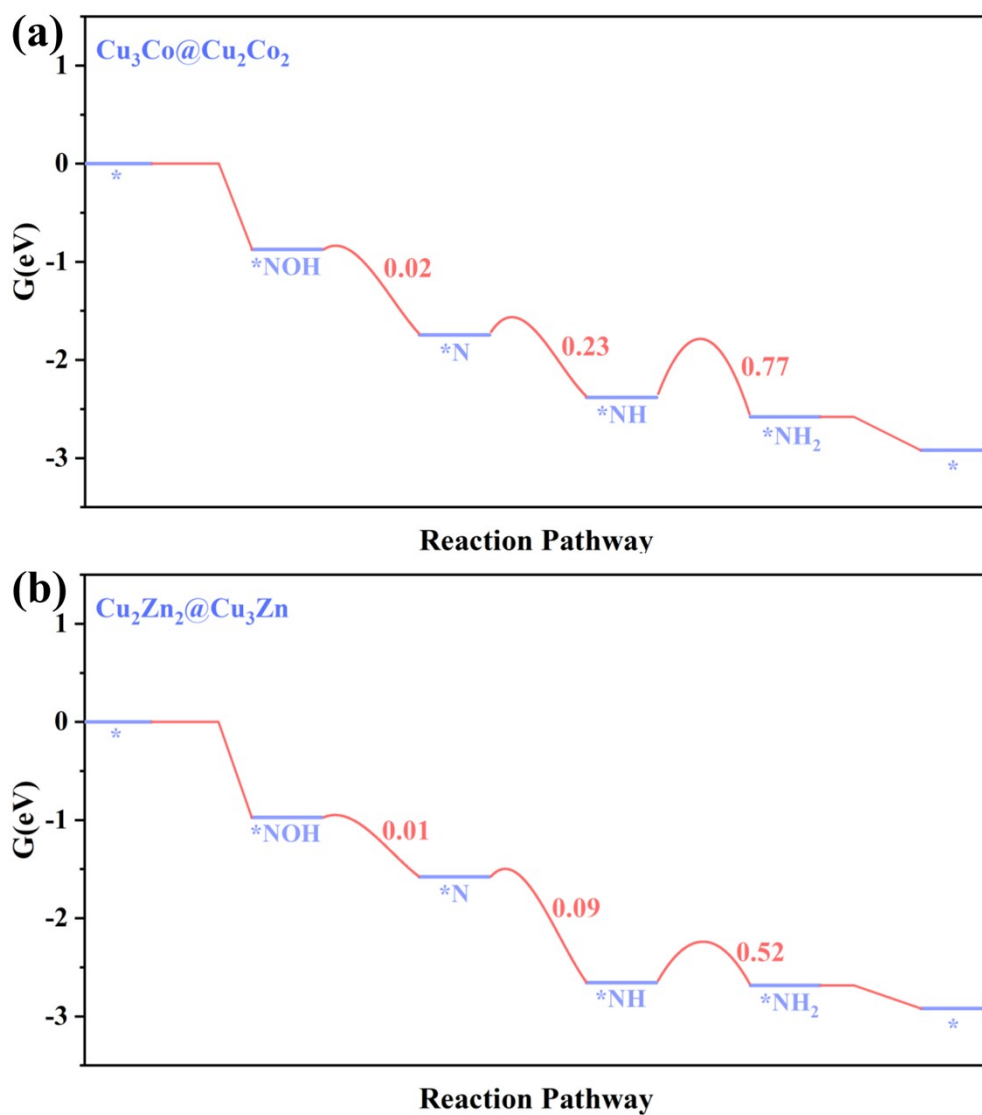


Figure S6. Kinetic barriers of the NORR for $\text{Cu}_3\text{Co}@Cu_2\text{Co}_2$ (a) and $\text{Cu}_2\text{Zn}_2@Cu_3\text{Zn}$ (b) along the Distal-O pathway.

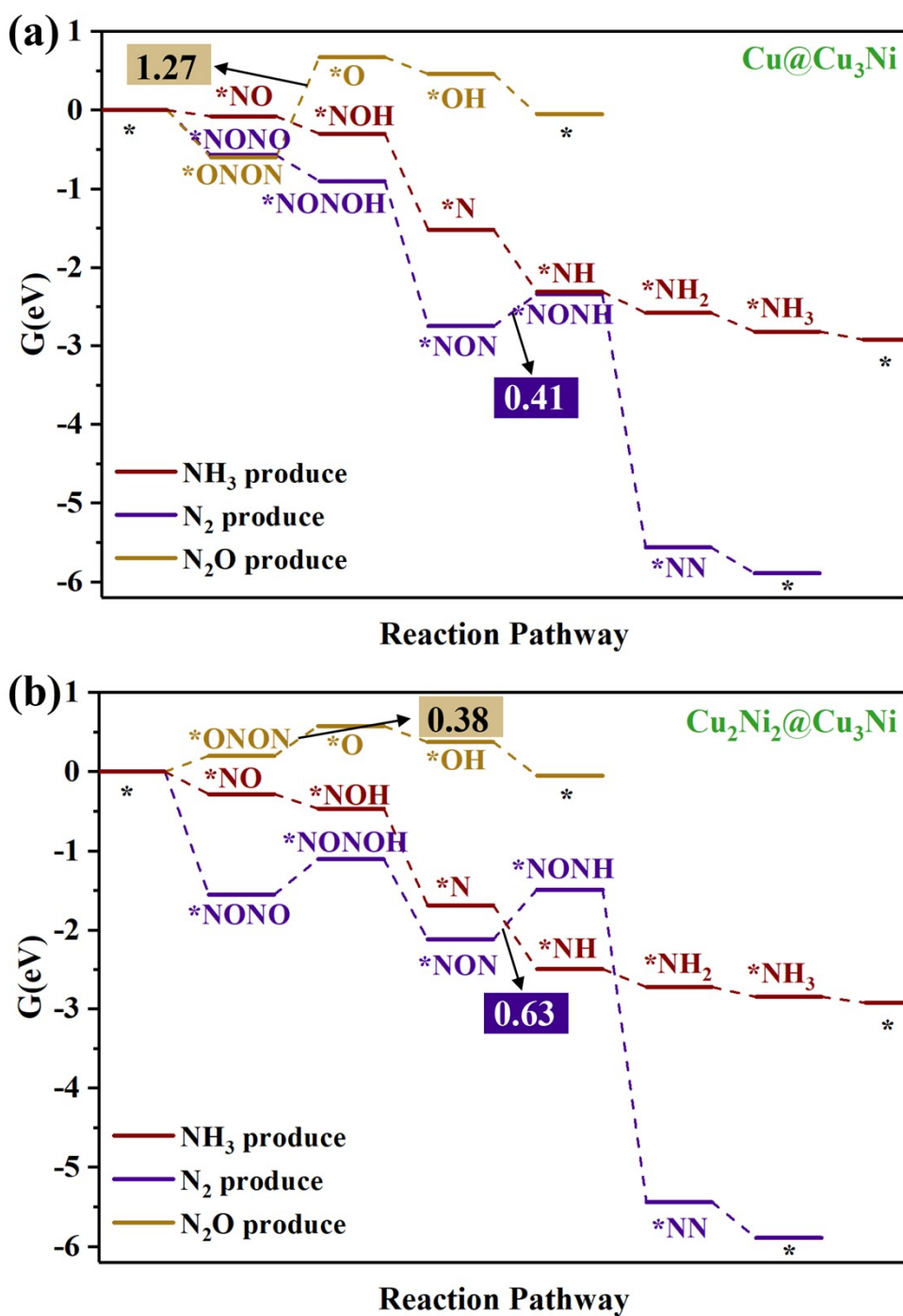


Figure S7. The reaction pathways of Cu@Cu₃Ni, Cu₂Ni₂@Cu₃Ni for NH₃ produce, N₂ produce, and N₂O produce. The protonation of *NO and *NH₂ do not change spontaneous processes of thermodynamics.

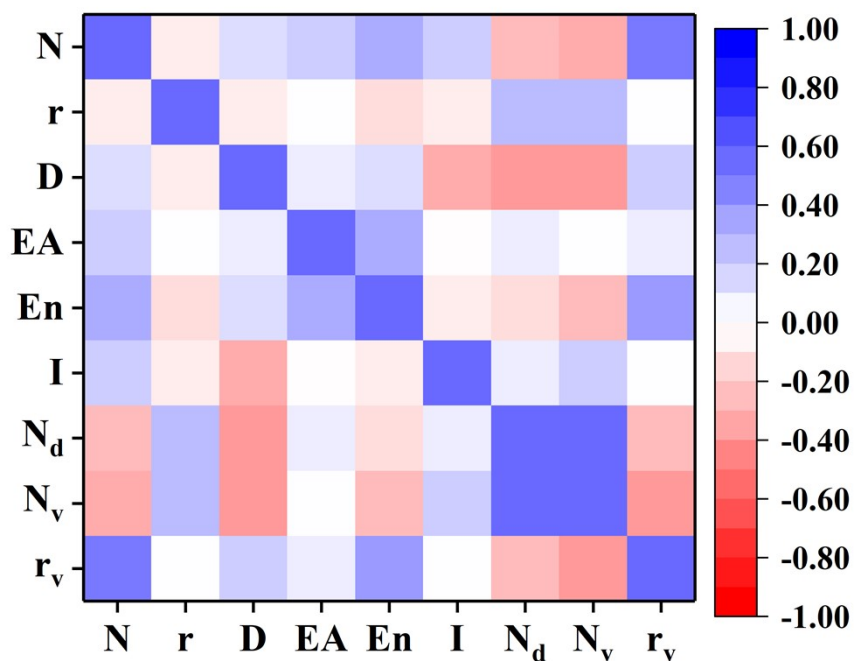


Figure S8. The heat map of the features by Pearson correlation coefficient analysis, including atomic number (N), atomic radius (r), dipole polarizability (D), electron affinity (EA), Pauling electronegativity (En), ionization potential (I), and the number of d electron (N_d), valence electron number (N_v), and van der Waals radius (r_v).

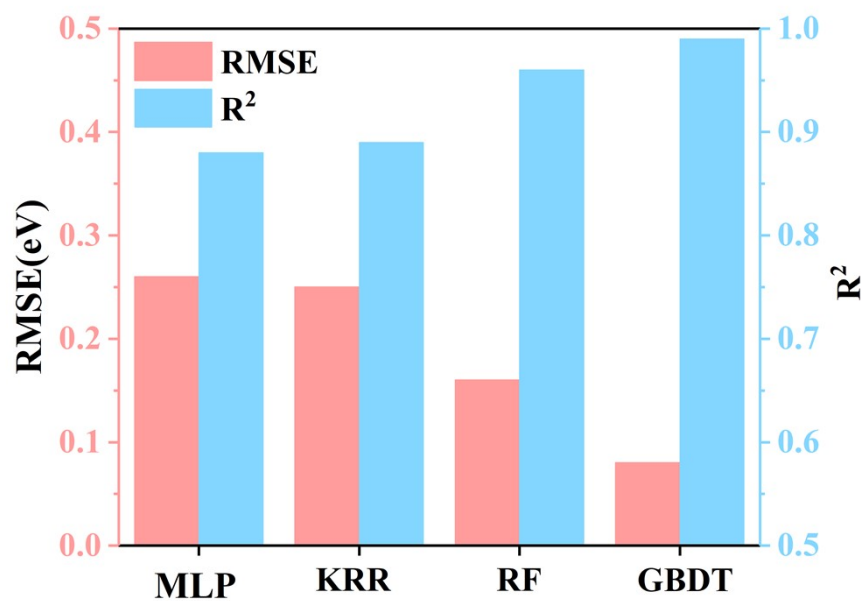


Figure S9. The RMSE and the R² score of 4 ML models (MLP, KRR, RF, and GBDT) on the train set.

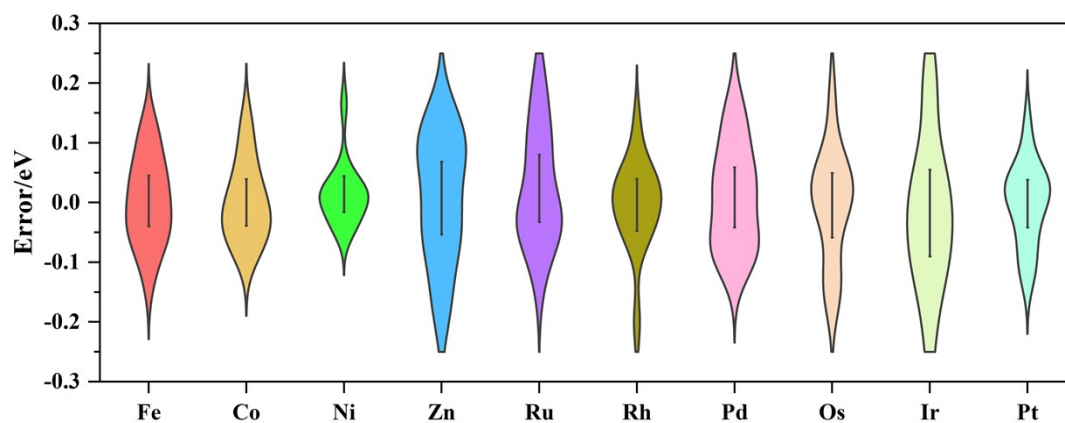


Figure S10. The violin plot of error distributions for each metal.

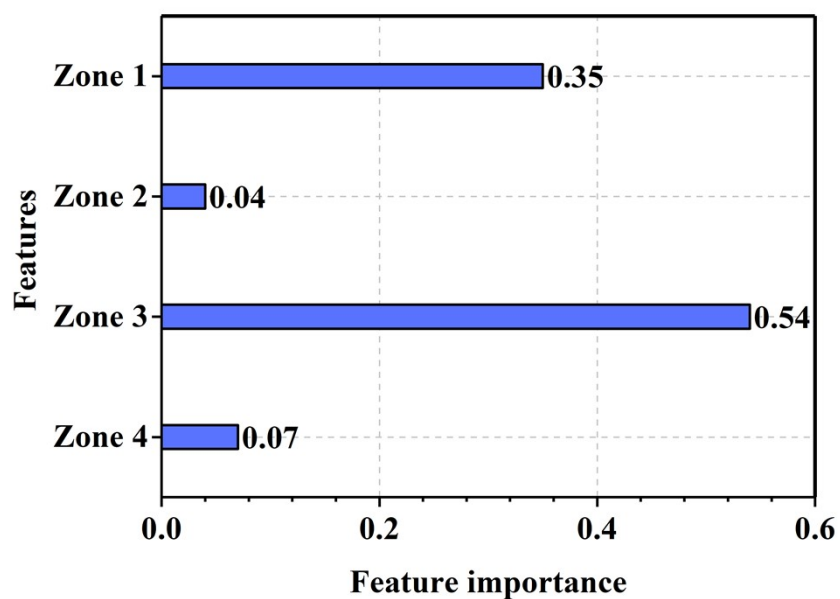


Figure S11. The feature importance analysis for the local environment of Zone 1, Zone 2, Zone 3, and Zone 4.

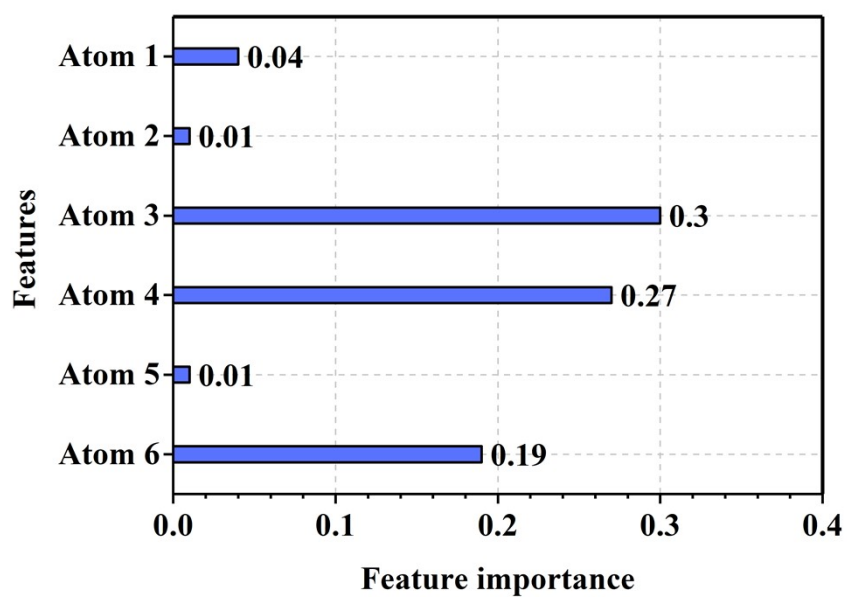


Figure S12. The feature importance analysis for the local environment of Atom 1, Atom 2, Atom 3, Atom 4, Atom 5, and Atom 6.

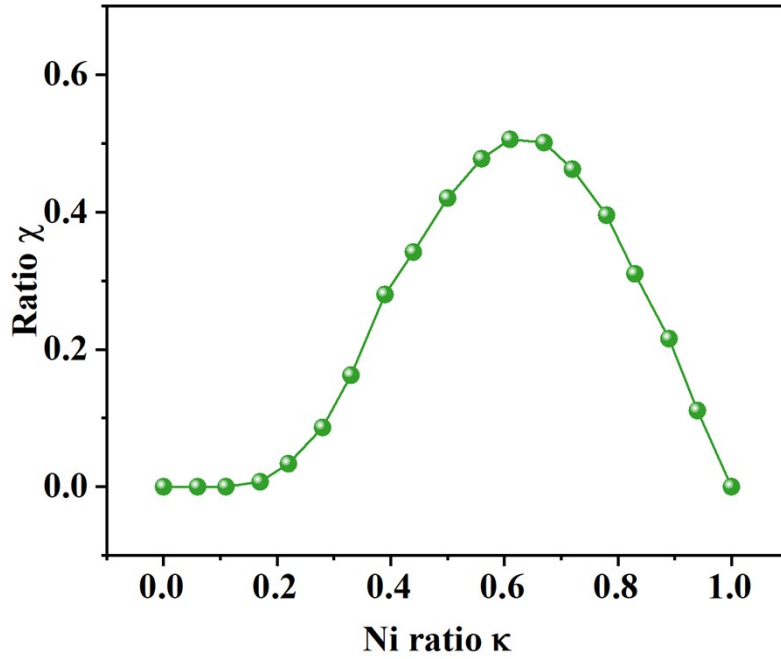


Figure S13. The ratio (χ) of the predicted $E_{\text{ads}}(*\text{N})$ ranging from 0.7 eV to 1.3 eV for every Ni ratio κ . We analyze the ratio of Ni (κ) in all CuNi alloy surfaces, and then for each ratio κ , we count the number of all surfaces (N_{κ}) and the number of the surface with the $E_{\text{ads}}(*\text{N})$ ranging from 0.7 eV to 1.3 eV (N). By these data, we calculate the ratio (χ) of the predicted $E_{\text{ads}}(*\text{N})$ ranging from 0.7 eV to 1.3 eV in all possible surfaces

for every Ni ratio κ , namely:

$$\chi = \frac{N}{N_{\kappa}}$$

Supplementary References

- 1 K. P. Murphy, *Machine learning: A probabilistic perspective*; MIT press, 2012.
- 2 S. K. Pal and S. Mitra, 1992.
- 3 G. Biau and E. Scornet, *Test*, 2016, **25**, 197-227.
- 4 J. H. Friedman, *Annals of statistics*, 2001, 1189-1232.
- 5 Y. Freund and L. Mason In *The alternating decision tree learning algorithm*, icml, 1999; pp 124-133.